Long-range ordering and representational analysis of the jarosites

A. S. Wills
Département de Recherche Fondamentale sur la Matière Condensée, SPSMS, CEA Grenoble, 38054 Grenoble, France
(Received 10 August 2000; published 24 January 2001)

The jarosites are the most studied family of *kagomé* antiferromagnets. Despite these works little is still known about the detailed causes of the observed magnetic structures. In this article representational analysis is used to determine the possible symmetry-allowed magnetic structures for the observed propagation vectors, and to examine their stability conditions. Refinements are presented of the magnetic structures of $AgFe_3(SO_4)_2(OD)_6$ and $(H_3O)V_3(SO_4)_2(OH)_6$. The steps required for these calculations and the refinement of the models against the neutron-diffraction data are detailed.

DOI: 10.1103/PhysRevB.63.064430 PACS number(s): 75.25.+z, 75.50.Ee

I. INTRODUCTION

Antiferromagnets with *kagomé* geometry have been the subject of much recent experimental and theoretical interest after predictions that at low temperature they could condense into exotic ground states.[1] The most studied *kagomé* systems are those based on the jarosite series $AB_3(SO_4)_2(OH)_6$ (where $A=Na^+$, K^+, Rb^+, Ag^+, H_3O^+, and $\frac{1}{2}Pb^{2+}$; $B=Fe^{3+}$, Cr^{3+}, and V^{3+}). Within this structure-type Néel long-range order,[2–6] highly fluctuating[6] and unconventional spin-glass[7–10,5] ground states have been observed. In the materials that possess long-range order, it is believed that the balance of energies required to stabilize nonconventional ordering is broken by the presence of further-neighbor exchange interactions.[6] Comparisons between the different possible structures are important as they yield direct information on the values of the exchange constants and other parameters that are required for their stability.

In the present paper the technique of representational analysis is used to calculate the basis functions of the group D_{3d}^5 magnetic representations for the observed (rather than typical) values of the propagation vector. These are used to classify and determine the possible magnetic structures, and to analyze the physical quantities that could be their cause. Particular attention is given to a discussion of the conjecture that single-ion effects play a role in defining the spin orientations in these materials.[3,4]

II. THE ALUNITE CRYSTAL STRUCTURE

In terms of their crystallography, the jarosites crystallize in the alunite structure [alunite itself is $KAl_3(SO_4)_2(OH)_6$].[11] As $B=Al^{3+}$ these compositions are nonmagnetic. The term jarosite, which specifically refers to the mineralogical family $AFe_3(SO_4)_2(OH)_6$, has now been applied more generally to distinguish the magnetic compositions with this structure, $B=Fe^{3+}$, Cr^{3+}, and V^{3+}.[2–6,12] The compositions within this family that show a transition to long-range Néel order are the subject of the following analysis.

The majority of the jarosites are described in the space group $R\bar{3}m$ and their crystal structure is displayed in Fig. 1. The exception is plumbojarosite $Pb_{0.5}Fe_3(SO_4)_2(OH)_6$, in which segregation of the Pb^{2+} ions into alternatively vacant and filled sites (experimentally observed occupations are 0.09 and 0.96, respectively) causes the *c* axis to be doubled; the remainder of the structure has no gross distortions away from the idealized structure.[13,14] In the alunite structure, the B^{3+} ions are coordinated by a distorted octahedron of four hyroxy and two sulfate oxygen atoms. These octahedra are joined by corner sharing to form the *kagomé* net. Within the sulfate layers between the *kagomé* layers the A^+ ions occupy 12 coordinate sites.

It is known that the jarosites are prone to nonstoichiometry on both the *A* and the *B* sites: up to 80% of the *A* cations can be replaced by H_3O^+, while a deficiency of Fe^{3+} is charge balanced by protonation of the hydroxy groups to form H_2O. This leads to an occupation of Fe^{3+} sites that is generally less than 100%, and typically in the range 83–93 %. An exception is the hydronium salt

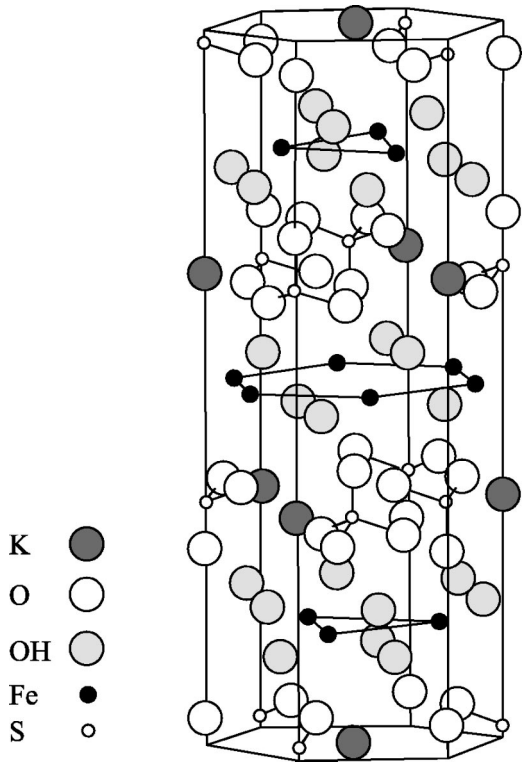

FIG. 1. The alunite crystal structure.

$(H_3O)Fe_3(SO_4)_2(OH)_6$, which can be prepared with an iron content of $\sim 97\%$.[7]

III. EXPERIMENT

The synthesis and full crystal structure refinement of $(H_3O)V_3(SO_4)_2(OH)_6$ will be described in a separate work.[15] Due to synthetic difficulties the unusual step was taken of using a protonated rather than a deuterated sample. As this paper is focused on the magnetic structures we will restrict the description of $(H_3O)V_3(SO_4)_2(OH)_6$ to the points necessary to refine the magnetic structure. Neutron-diffraction data from $(H_3O)V_3(SO_4)_2(OH)_6$ were collected using neutrons of wavelength 2.4 Å using the D20 diffractometer of the Institut Laue-Langevin. The sample was held in a vanadium can and data collected above and below an ordering temperature $T_c \simeq 21$ K. The large angular range of the diffractometer allowed the collection of data over a sufficient Q range for the analysis of both nuclear and magnetic structures. Refinement of the $R\bar{3}m$ nuclear structure was carried out using the PC translation of the GSAS suite.[16] The magnetic structure factors were then calculated using the GENLES routine of the GSAS suite, while the symmetry and orientations of the magnetic moments were controlled and refined separately by the program SARA*h*-Refine for GSAS.[17] Refinement was made *directly* of the basis vector mixing coefficients within the representation under testing using a reverse-Monte Carlo (RMC) algorithm.[18] This technique examines a greater range of phase space than is stable using conventional least-squares refinement techniques, and so allows the investigation and location of other minima in the refinement variable hyperspace. As magnetic structure determination is frequently hindered by limited data sets and the possibilities of several magnetic structures with identical structure factors, this technique gives more information on the quality of the refinement and the uniqueness of the solutions. Once a minimum has been found, optimization using least squares can be carried out. However, in cases involving only two basis vectors, a RMC refinement made using 100 cycles was not found to be further improved by least-squares optimization.

In the following refinements, the mixing coefficients for the basis vectors of each irreducible representation were constrained to have random values between $+1$ and -1, such that the sum of their magnitudes was of modulus unity. The orientations of all the moments in the complete magnetic cell for this random spin configuration, which lies within the possible symmetry-allowed structures of the chosen representation, were calculated from these. During each RMC cycle three least-squares cycles were made in order to refine the optimum magnitude of the magnetic moments, the only variable allowed to refine during the RMC cycles. This was constrained to be equal for all the atoms in the magnetic cell.

The neutron-diffraction data presented here, collected using neutrons of wavelength 2.52 Å from $AgFe_3(SO_4)_2(OH)_6$ at 1.5 K have been previously reported in Ref. 5.

IV. CASE OF k=0

A. Decomposition of the magnetic representation and the basis vectors

In the hexagonal setting the magnetic Fe^{3+} ions are found on the $9d$ sites. For these sites the decomposition of the magnetic representation according to Eq. (A16) is

$$\Gamma = 1\Gamma_1^{(1)} + 0\Gamma_2^{(1)} + 2\Gamma_3^{(1)} + 0\Gamma_4^{(2)} + 0\Gamma_5^{(2)} + 3\Gamma_6^{(2)}. \quad (1)$$

Landau theory requires that only one representation can be involved in a critical transition, and so with this constraint there are only three possible magnetic structures for this **k**. These representations correspond to those that have a nonzero contribution: the representations Γ_1, Γ_3, and Γ_6.

The basis vectors for these representations calculated according to Eq. (A17) are given in Table I. The atomic sites are labeled following the convention given in Sec. A 3. These basis vectors have varied forms and the types of magnetic structures to which they correspond will now be discussed.

Representations Γ_1 and Γ_3 are one dimensional. They therefore correspond to simple magnetic structures in which the atomic moments are orientated along particular crystallographic axes. It is noteworthy that both ψ_1 and ψ_2 correspond to the so-called ''$q=0$'' spin structure:[19–21] a 120° spin structure with the total spin on any given triangle plaquette being $\Sigma_i S_i = 0$ (Fig. 2). While the two spin structures are related by a 60° reorientation of spins, the two representations differ in that Γ_3 allows the introduction of an out-of-plane component, which corresponds to ψ_3. The combination of the two basis functions ψ_2 and ψ_3 creates a so-called ''umbrella structure,'' in which the degree of out-of-plane canting is a refinement variable.

Representation Γ_6 is two dimensional and is repeated three times. It therefore corresponds to a six basis vector magnetic structure. As the general solution involves any linear combination of these six basis vectors we cannot ascribe to this representation a simple structure. However, there are relations between the basis vectors and these will simplify the refinement of the mixing coefficients $\psi_5^* = \psi_7$, $\psi_4^* = \psi_8$, and $\psi_6^* = \psi_9$.

As the atomic spins are real entities, in the case of complex basis vectors it is necessary to introduce the corresponding basis vectors of the propagation vector $-\mathbf{k}$ in order to make the summation of the two components real. This construction is easily explained if we examine the translation properties of the magnetic moments. The axial vector that describes the moment at position $\mathbf{r}_i$ can be expressed in terms of that at $\mathbf{r}_j$ by the addition of the phase factor $\exp(2\pi\mathbf{k}\cdot\Delta\mathbf{r})$,

$$S(\mathbf{r}_i) = S(\mathbf{r}_j)\cdot\exp(2\pi\mathbf{k}\cdot\Delta\mathbf{r}). \quad (2)$$

Here, the positions of the two atoms are related by a lattice translation $\Delta\mathbf{r}$,

$$\mathbf{r}_i = \mathbf{r}_j + \Delta\mathbf{r}. \quad (3)$$

TABLE I. The basis functions of the irreducible group representations (IGR) of the space group $R\bar{3}m$ (point group D_{3d}^5) appearing in the magnetic representation with $\mathbf{k}=0$.

IR	Basis vector	Atom 1			Atom 2			Atom 3		
		m_x	m_y	m_z	m_x	m_y	m_z	m_x	m_y	m_z
Γ_1	ψ_1	1	1	0	-1	0	0	0	-1	0
Γ_3	ψ_2	1	-1	0	1	2	0	-2	-1	0
	ψ_3	0	0	1	0	0	1	0	0	1
Γ_6	ψ_4	1	0	0	0	$-\frac{1}{2}-\frac{\sqrt{3}}{2}i$	0	$\frac{1}{2}-\frac{\sqrt{3}}{2}i$	$\frac{1}{2}-\frac{\sqrt{3}}{2}i$	0
	ψ_5	0	1	0	$\frac{1}{2}+\frac{\sqrt{3}}{2}i$	$\frac{1}{2}+\frac{\sqrt{3}}{2}i$	0	$-\frac{1}{2}+\frac{\sqrt{3}}{2}i$	0	0
	ψ_6	0	0	1	0	0	$-\frac{1}{2}-\frac{\sqrt{3}}{2}i$	0	0	$-\frac{1}{2}+\frac{\sqrt{3}}{2}i$
	ψ_7	0	1	0	$\frac{1}{2}-\frac{\sqrt{3}}{2}i$	$\frac{1}{2}-\frac{\sqrt{3}}{2}i$	0	$-\frac{1}{2}-\frac{\sqrt{3}}{2}i$	0	0
	ψ_8	1	0	0	0	$-\frac{1}{2}+\frac{\sqrt{3}}{2}i$	0	$\frac{1}{2}+\frac{\sqrt{3}}{2}i$	$\frac{1}{2}+\frac{\sqrt{3}}{2}i$	0
	ψ_9	0	0	-1	0	0	$\frac{1}{2}-\frac{\sqrt{3}}{2}i$	0	0	$\frac{1}{2}+\frac{\sqrt{3}}{2}i$

Omitting the subscript of the atom, the atomic vector for an atom in the nth cell related to that in the *zero*th cell by translation $\mathbf{t}_n$ is then given by[22]

$$S_n^{\mathbf{k}}=S_0^{\mathbf{k}}e^{2\pi i\mathbf{k}\cdot\mathbf{t}_n}+S_0^{-\mathbf{k}}e^{-2\pi i\mathbf{k}\cdot\mathbf{t}_n}. \tag{4}$$

As for both $\mathbf{k}=000$ and $\mathbf{k}=00\frac{3}{2}$ the vectors $\mathbf{k}$ and $-\mathbf{k}$ are identical, we have $-\mathbf{k}=\mathbf{k}$, and so

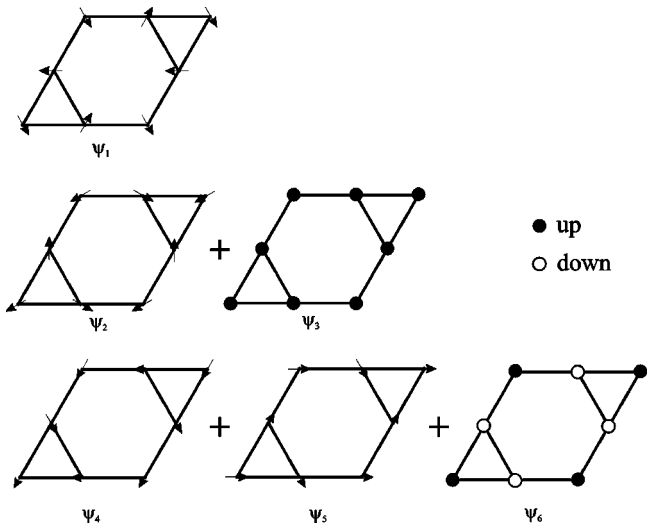

FIG. 2. Moment directions for the basis vectors ψ_1–ψ_6. ψ_1 and ψ_2 are related by a rotation of 60°; ψ_4 and ψ_5 are related by a rotation of 120°.

$$S_n^{\mathbf{k}}=(S_0^{\mathbf{k}}+S_0^{-\mathbf{k}})e^{2\pi i\mathbf{k}\cdot\mathbf{t}_n} \tag{5}$$

A further simplification arises from the fact that the addition of the $-\mathbf{k}$ contribution corresponds to the addition of the conjugate of $\mathbf{k}$,[23,24] i.e.,

$$S_0^{-\mathbf{k}}=S_0^{\mathbf{k}*}. \tag{6}$$

We therefore obtain

$$S_n^{\mathbf{k}}=2\,\mathrm{Re}(S_0^{\mathbf{k}})\cos(2\pi i\mathbf{k}\cdot\mathbf{t}_n)+i2\,\mathrm{Re}(S_0^{\mathbf{k}})\sin(2\pi i\mathbf{k}\cdot\mathbf{t}_n). \tag{7}$$

For both $\mathbf{k}=000$ and $\mathbf{k}=00\frac{3}{2}$ the sine component vanishes under the centering translations of the nonprimitive cell, or integer translations of the crystallographic cell, and so Eq. (7) reduces to

$$S_n^{\mathbf{k}}=2\,\mathrm{Re}(S_0^{\mathbf{k}})\cos(2\pi i\mathbf{k}\cdot\mathbf{t}_n). \tag{8}$$

Therefore, when considering the translational properties of the magnetic moments described by the complex basis vectors associated with Γ_6, it is sufficient to add their complex conjugate in order to arrive at real values for the atomic moments.

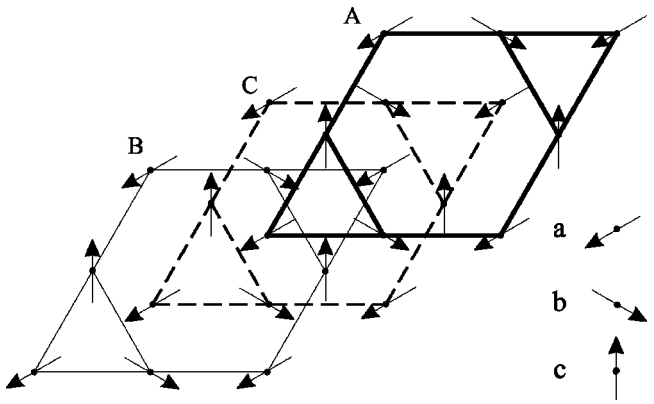

FIG. 3. In-plane magnetic structure of $KFe_3(CrO_4)_2(OD)_6$ and $KCr_3(SO_4)_2(OD)_6$ with the three Bravais sublattices a,b,c of the *kagomé A* layer. The layers have the hexagonal stacking sequence $\ldots ABC \ldots$

B. The magnetic structures of $KFe_3(CrO_4)_2(OD)_6$ and $KCr_3(SO_4)_2(OD)_6$

Both $KFe_3(CrO_4)_2(OD)_6$ and $KCr_3(SO_4)_2(OD)_6$ order with the propagation vector $\mathbf{k}=000$. Inspection of the magnetic structure for $KFe_3(CrO_4)_2(OD)_6$ proposed by Townsend quickly indicates that it does not correspond to any combination of the basis vectors given in Table I and so is forbidden according to group theory. However, the observation of a small ferromagnetic component at low temperature does allow the true magnetic structure to be deduced given the assumption of antiferromagnetic nearest-neighbor exchange, as evidenced by bulk susceptibility measurements.[2] This is possible as ferromagnetism is compatible only with ordering under the representation Γ_3, which permits a ferromagnetic component parallel to the c axis. The spin structure therefore corresponds to an umbrella mode in which the in-plane components of the moments are fixed along the directions shown in Fig. 3.

Recent observation of a small ferromagnetic component at low temperatures in the $S=\frac{3}{2}$ chromium jarosite $KCr_3(SO_4)_2(OD)_6$ by NMR[25] indicates that it too orders with the same umbrella spin structure.

V. CASE OF $\mathbf{k}=00\frac{3}{2}$

A. Decomposition of the magnetic representation and the basis vectors

The decomposition of the magnetic representation for this propagation vector is

$$\Gamma = 0\Gamma_1^{(1)} + 2\Gamma_2^{(1)} + 0\Gamma_3^{(1)} + 1\Gamma_4^{(2)} + 3\Gamma_5^{(2)} + 0\Gamma_6^{(2)}. \quad (9)$$

The symmetries of the representations are such that the basis vectors of the representation $\Gamma_2(\mathbf{k}=00\frac{3}{2})$ are identical to those of $\Gamma_3(\mathbf{k}=0)$, and that those of $\Gamma_4(\mathbf{k}=00\frac{3}{2})=\Gamma_1(\mathbf{k}=000)$ and of $\Gamma_5(\mathbf{k}=00\frac{3}{2})=\Gamma_6(\mathbf{k}=0)$. Because of this relation we will continue to use the same basis vectors and numbering scheme presented in Table I.

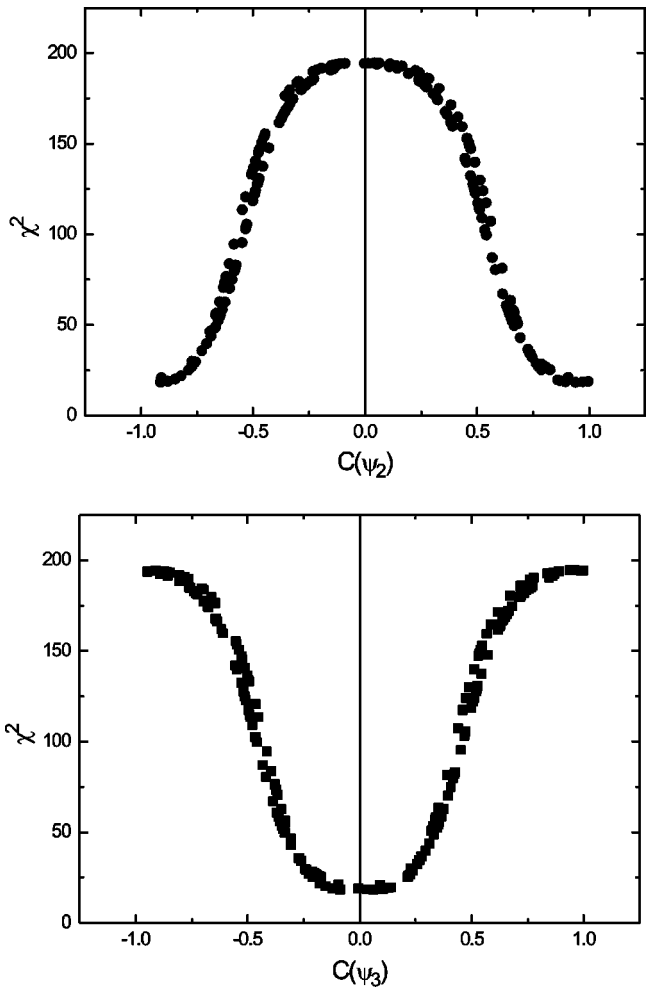

FIG. 4. χ^2 as a function of the basis vector coefficients $C(\psi_1)$ and $C(\psi_2)$ during the refinement of the magnetic structure of $AgFe_3(SO_4)_2(OD)_6$ at 1.5 K.

While representational analysis for both of these propagation vectors leads to the same symmetry-allowed basis vectors, we must remember that the different propagation vectors will lead to different magnetic structures. In particular, the reversal of the moments related by the lattice translations of the primitive cell for the $\mathbf{k}=00\frac{3}{2}$ prevents the formation of a net moment for any spin structure.

B. Refinement of the magnetic structure of $AgFe_3(SO_4)_2(OD)_6$

The collected low-temperature neutron-diffraction data were found to be most compatible with a magnetic structure described by the basis vectors ψ_2 and ψ_3 of the representation $\Gamma_2(\mathbf{k}=00\frac{3}{2})$. Figure 4 displays the value of χ^2 as a function of the mixing coefficients $C(\psi_2)$ and $C(\psi_3)$. The best value of χ^2 corresponds to the coefficients $C(\psi_1)=0.99\pm0.05$ and $C(\psi_2)=0.01\pm0.05$, and the time-reversed $C(\psi_1)=-0.99\pm0.05$ and $C(\psi_2)=-0.01\pm0.05$. The refined structure is therefore coplanar and the contribution from out-of-plane canting is zero within the error limits of these data. The final refined profile is presented in Fig. 5 and the refined magnetic structure in Fig. 6. The final values

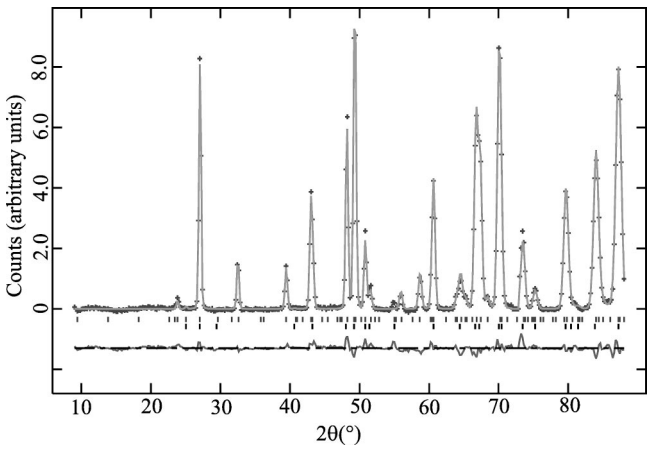

FIG. 5. Experimental and calculated diffraction patterns for $AgFe_3(SO_4)_2(OD)_6$ at 1.5 K.

of χ^2 and R_{wp} are 18.9 and 2.4 %, respectively; the size of the Fe^{3+} moment refined to 3.50 (3)μ_B.

C. Refinement of the magnetic structure of $(H_3O)V_3(SO_4)_2(OH)_6$

The collected data are only well modeled by a strucure based on $\Gamma_5(\mathbf{k}=00\frac{3}{2})$. As its basis vectors are split into three unique vectors and their complex conjugates, only the contributions from the basis vectors ψ_4, ψ_5, and ψ_6 are required in order to generate all the possible magnetic structures associated with this representation. In fact, the out-of-plane contribution from the ψ_6 refined to zero and the data are well described with only ψ_4 and ψ_5. The values of χ^2 against the various values of the $C(\psi_4)$ and $C(\psi_5)$ are displayed in Fig. 7, the final refined diffraction pattern in Fig. 8, and the magnetic structure is presented in Fig. 9. The final values of χ^2 and R_{wp} are 0.0013 and 1.07 %, respectively; the size of the moment on the vanadium atom refined to 2.18 (3)μ_B, which compares reasonably with the spin-only Néel value of $gS\mu_B=2\mu_B$ if the g factor for V^{3+} is assumed to be 2. The unusually low values of χ^2 are due to the high incoherent background contribution to the scattering due to the protons in the sample.

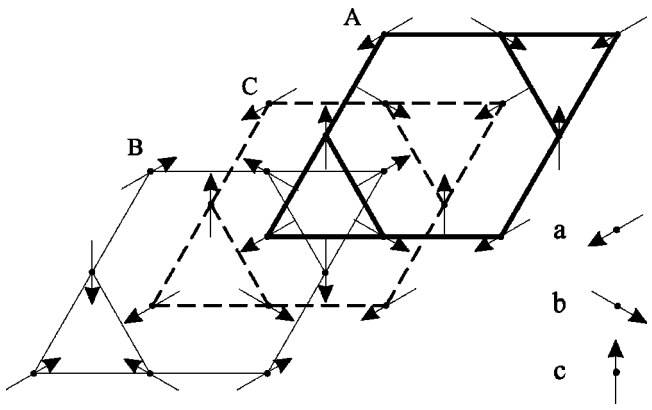

FIG. 6. Magnetic structure of $AgFe_3(SO_4)_2(OD)_6$ with the three Bravais sublattices a,b,c of the *kagomé A* layer.

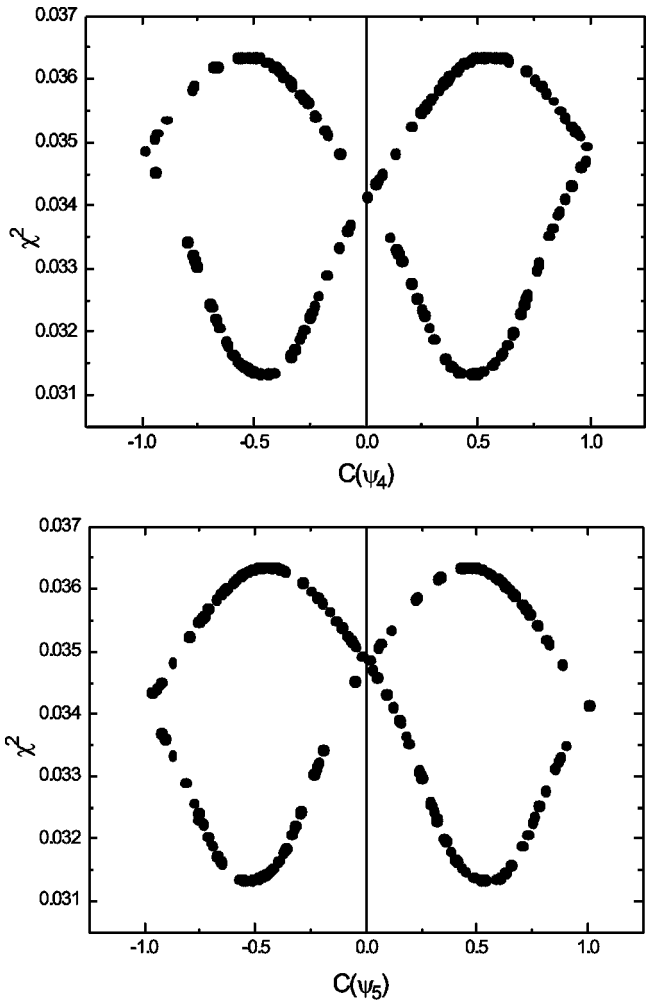

FIG. 7. χ^2 as a function of the basis vector coefficients ψ_4 and ψ_5 during the refinement of the magnetic structure of $(H_3O)V_3(SO_4)_2(OH)_6$ at 1.5 K.

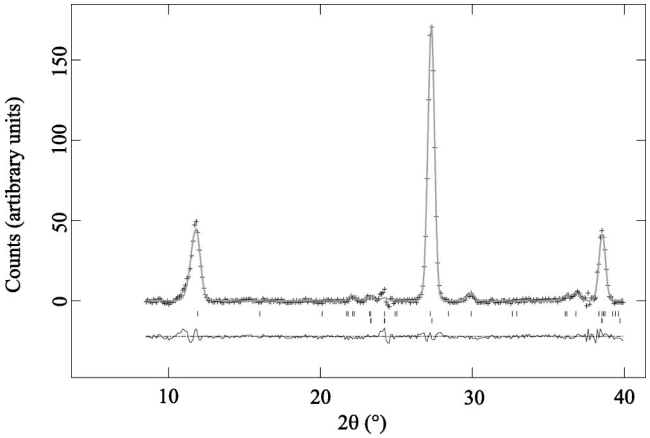

FIG. 8. Experimental and calculated diffraction patterns for $(H_3O)V_3(SO_4)_2(OH)_6$ at 1.5 K with the three Bravais sublattices a,b,c of the *kagomé A* layer.

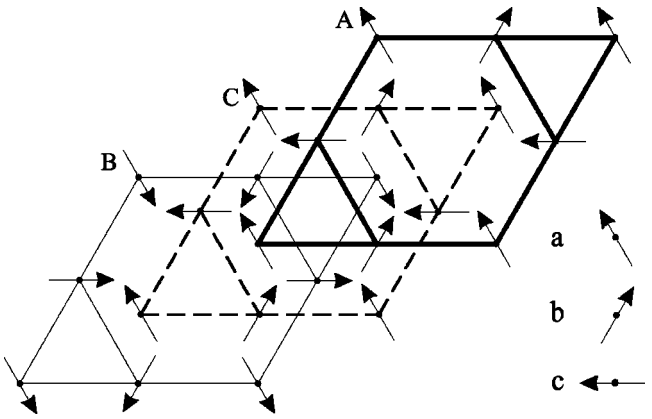

FIG. 9. Magnetic structure of $(H_3O)V_3(SO_4)_2(OH)_6$ with $C(\psi_4)=0.50$, $C(\psi_5)=0.50$.

The refined values of the coefficients are $C(\psi_4)$ 0.45 ± 0.05, $C(\psi_5)$ 0.55 ± 0.05, and $C(\psi_4)=-0.45\pm 0.05$, $C(\psi_5)=-0.55\pm 0.05$.

VI. ANALYSIS OF THE ENERGIES OF THE OBSERVED STRUCTURES

Given that the magnetic structures of the different irreducible representations are eigenvalues of the exchange Hamiltonian, comparison of the different possible spin configurations gives information on the values of the exchange constants required to stabilize them. In the following section the in-plane and interplane couplings in the observed magnetic structures of $KCr_3(SO_4)_2(OD)_6$, $AgFe_3(SO_4)_2(OD)_6$, and $(H_3O)V_3(SO_4)_2(OH)_6$ are examined separately. The expansions for the exchange energies have been tabulated in Tables II–IV in terms of the nearest-neighbor (J) and next-nearest-neighbor (J') exchange couplings for both intra- and interplane interactions. The exchange energy for spin i is defined by

$$E_i=-\sum_j J_{i,j}\mathbf{S}_i\cdot\mathbf{S}_j. \tag{10}$$

In the case of ordering under the repeated first-order representations $\Gamma_1(\mathbf{k}=000)$ or $\Gamma_4(\mathbf{k}=00\frac{3}{2})$, the assumption has been made that the moments lie in the *kagomé* plane. This is not the case for all the compositions as $KCr_3(SO_4)_2(OD)_6$ and $KFe_3(CrO_4)_2(OD)_6$ display a small spontaneous moment. Such a canting cannot be ascribed to simple intraplane or interplane exchange, and therefore is likely to be the result of some small single-ion effects or a Dzyaloshinsky-Moriya coupling,[26] rather than the superexchange interactions examined here. The weakness of the observed spontaneous moments indicates also that this canting is small and that its effects on the Hamiltonians involved can be ignored at the level of these calculations.

TABLE II. The expansion of the intraplane exchange energies for the 120° and $(H_3O)V_3(SO_4)_2(OH)_6$ orderings.

Moment	120°	$(H_3O)V_3(SO_4)_2(OH)_6$
a	$2J+2J'$	$-2J-2J'$
b	$2J+2J'$	0
c	$2J+2J'$	0
Total	$6J+6J'$	$-2J-2J'$

TABLE III. The expansion of the interplane exchange energies for the 120° structure for the propagation vectors $\mathbf{k}=000$ and $\mathbf{k}=00\frac{3}{2}$.

Moment	$\mathbf{k}=000$	$\mathbf{k}=00\frac{3}{2}$
a	$J_{interplane}-3J'_{interplane}$	$-J_{interplane}+3J'_{interplane}$
b	$J_{interplane}-3J'_{interplane}$	$-J_{interplane}+3J'_{interplane}$
c	$J_{interplane}-3J'_{interplane}$	$-J_{interplane}+3J'_{interplane}$
Total	$3J_{interplane}-9J'_{interplane}$	$-3J_{interplane}+9J'_{interplane}$

A. Zero-energy moments and additional degeneracies in $(H_3O)V_3(SO_4)_2(OH)_6$

Inspection of Tables II and IV reveals that the observed magnetic structure of $(H_3O)V_3(SO_4)_2(OH)_6$ is extraordinary. The expansions for the exchange energy show that the three Bravais sublattices are separated into two classes. The first, labeled a in Fig. 10, experiences an intraplane exchange energy of

$$E=-2J-2J' \tag{11}$$

and an interplane exchange energy of

$$E_{interplane}=J_{interplane}+3J'_{interplane}. \tag{12}$$

Those with labels b and c show a much more unusual energy profile as despite a nonzero exchange field being present at their sites, their orientations are such that they possess zero intraplane exchange energy, even to the approximation of next-nearest neighbors. The only nonzero-energy term appears to be from the interplane coupling to the next-nearest neighbors

$$E_{interplane}=3J'_{interplane}. \tag{13}$$

In addition to the nearest-neighbor exchange energies cancelling for these moments, the b and c sites have additional localized and extended degeneracies that may be expected to affect the low-temperature physics. The localized modes are demonstrated in Fig. 10 and correspond to a single

TABLE IV. The expansion of the interplane exchange energies for the structure observed in $(H_3O)V_3(SO_4)_2(OH)_6$ for the propagation vectors $\mathbf{k}=000$ and $\mathbf{k}=00\frac{3}{2}$.

Moment	$\mathbf{k}=000$	$\mathbf{k}=00\frac{3}{2}$
a	$-3J'_{interplane}$	$J_{interplane}+3J'_{interplane}$
b	$-3J'_{interplane}$	$3J'_{interplane}$
c	$-3J'_{interplane}$	$3J'_{interplane}$
Total	$-9J'_{interplane}$	$J_{interplane}+9J'_{interplane}$

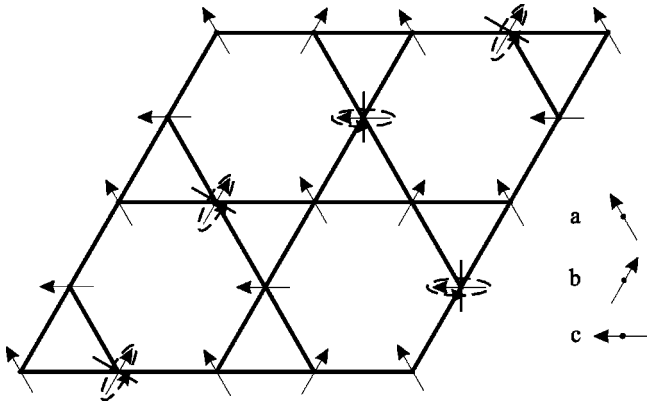

FIG. 10. Localized zero-energy excitations in $(H_3O)V_3(SO_4)_2(OH)_6$ involving the continuous rotation of one *b* or *c* moment per triangle.

b or *c* moment per triangle spinning about the axis defined by the mirror plane relating the two remaining moments of the triangle. This motion is continuously degenerate as it costs zero intraplane and interplane exchange energy, to the next-nearest-neighbor level of approximation. These modes do however interact if they are present at the distance of further-neighbor atoms or closer.

Extended zero-energy modes are also possible, at the nearest-neighbor level of approximation, in which lines of *b* and *c* moments rotate simultaneously about the axis defined by the *a* moments, as shown in Fig. 11.

B. Interplane exchange in $(H_3O)V_3(SO_4)_2(OH)_6$

Making the assumption that intra- and interplane exchange are uncorrelated, comparisons between the structure of $(H_3O)V_3(SO_4)_2(OH)_6$ with the possible and the observed propagation vectors $\mathbf{k}=000$ and $\mathbf{k}=00\frac{3}{2}$ gives information on the interplane exchange energies: the $\mathbf{k}=000$ and $\mathbf{k}=00\frac{3}{2}$ structures are stable if

$$-18J'_{interplane}<J_{interplane} \tag{14}$$

and

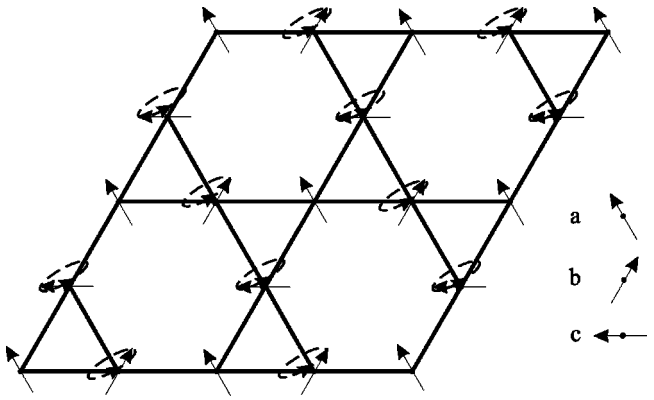

FIG. 11. Extended zero-energy excitations in $(H_3O)V_3(SO_4)_2(OH)_6$ involving the simultaneous rotation of lines of *b* and *c* moments.

$$-18J'_{interplane}>J_{interplane}, \tag{15}$$

respectively. As the nearest-neighbor exchange is typically far stronger than the next-nearest exchange, it is useful to examine these relations in the limit of zero next-nearest-neighbor exchange, $J'_{interplane}=0$. This then shows that the $\mathbf{k}=000$ structure is stabilized by ferromagnetic interactions, while the $\mathbf{k}=00\frac{3}{2}$ is stabilized by antiferromagnetic interactions.

C. Intraplane exchange in $AgFe_3(SO_4)_2(OD)_6$ and $(H_3O)V_3(SO_4)_2(OH)_6$

Comparison of the total intraplane exchange energies given in Table II indicates that the coplanar 120° ordering is stabilized if the inequality

$$J<J' \tag{16}$$

is satisfied. While conversely, the structure observed in $(H_3O)V_3(SO_4)_2(OH)_6$ is stabilized if

$$J>J'. \tag{17}$$

In the $J'=0$ limit, this shows that the 120° structures of the types observed in $AgFe_3(SO_4)_2(OD)_6$ and $KCr_3(SO_4)_2(OD)_6$ are stabilized by antiferromagnetic nearest-neighbor intraplane exchange, while that of $(H_3O)V_3(SO_4)_2(OH)_6$ is stabilized by ferromagnetic nearest-neighbor exchange.

D. Interplane exchange in $AgFe_3(SO_4)_2(OD)_6$ and $KCr_3(SO_4)_2(OD)_6$

Continuing the comparison for the 120° spin structures with the propagation vectors $\mathbf{k}=000$ and $\mathbf{k}=00\frac{3}{2}$ indicates that the $\mathbf{k}=000$ ordering is stabilized if

$$J_{interplane}<3J'_{interplane} \tag{18}$$

and conversely, that with the propagation vector $\mathbf{k}=00\frac{3}{2}$ by

$$J_{interplane}>3J'_{interplane}. \tag{19}$$

In the limit of zero next-nearest-neighbor interactions, we find that the $\mathbf{k}=000$ spin structure is stabilized by antiferromagnetic nearest-neighbor interplane exchange, in agreement with the proposal of Lee *et al.*[6] That with the propagation vector $\mathbf{k}=00\frac{3}{2}$ is stabilized by ferromagnetic nearest-neighbor interplane exchange.

VII. DISCUSSION

The determination of the magnetic structures of *kagomé* antiferromagnets features a special difficulty due to the vertex sharing exchange geometry: for any given value of the propagation vector the nearest-neighbor exchange is an insufficient criterion to stabilize a single magnetic structure, and a large number of possibilities with equal nearest-neighbor exchange energy exist. Representational analysis is especially useful in this case as it reduces greatly the number

of possible magnetic structures. Indeed, in the jarosites for both propagation vectors we find that there are only three ordering patterns possible for the ions of a *kagomé* layer: a 120° structure, an umbrella mode, and a more complex structure. Of these, at present only magnetic structures corresponding to the umbrella and the complex structures are observed.

The analyses presented clearly support previous work[6] that proposed that interplane interactions play an important role in the stabilization of the observed magnetic structures. This is particularly well demonstrated by the different propagation vectors of $AgFe_3(SO_4)_2(OD)_6$ and $KFe_3(CrO_4)_2(OD)_6$, systems where the only significant change in terms of the magnetism is the substitution of the XO_4^{2-} ion.

Recent neutron-diffraction measurements have shown that magnetic ordering in samples of $KFe_{3-x}Al_y(SO_4)_2(OD)_6$ involves the formation of an intermediate phase where the moments have an umbrella structure, and that at lower temperature a second transition occurs in which the moments collapse into the *kagomé* plane.[27] The absence of an out-of-plane component at low temperature in $KFe_3(SO_4)_2(OH)_6$ has been confirmed by neutron-diffraction studies made with full polarization analysis on a natural sample.[28] As yet, the physical properties responsible for these structures are not certain, but the group-theory arguments given here endorse suggestions[4] that the orientations of the moments along particular crystallographic directions in the observed ''$q=0$'' structures are a result of single-ion effects. However, they indicate that rather than simply defining the specific spin directions in the *kagomé* plane, a more indirect mechanism can occur, one in which the presence of an out-of-plane canting fixes, because of the symmetry of the basis vectors, the directions of the inplane components.

An important consequence of the tilting of the coordination octahedra around the *B* atoms is that an Ising-type anisotropy will give rise to an out-of-plane component to the moments. The second transition that involves a collapse of the moments into the plane may therefore be either the result of a diminution in this anisotropy, or the increase in some other influence that pushes the moments into the *kagomé* plane. The latter is unlikely to involve an order-by-disorder mechanism[29–31] as this operates at temperatures that are generally far lower that *J*, which is of the order of 40 and 15 K in the iron and chromium jarosites, respectively.[5,6,32] There is no apparent reason for this transition to involve a symmetry-breaking transition to the singly repeated first-order representations $\Gamma_1(\mathbf{k}=000)$ or $\Gamma_4(\mathbf{k}=00\frac{3}{2})$, rather than remaining within representation $\Gamma_3(\mathbf{k}=000)$ or $\Gamma_2(\mathbf{k}=00\frac{3}{2})$, as both these in-plane 120° structures have the same exchange energies. Accordingly, it may be the presence of a canting at high temperatures that continues to define the directions of the moments at low temperature, even when the canting is absent.

The magnetic structure determined for $(H_3O)V_3(SO_4)_2(OH)_6$ is intriguing as it cannot be explained in terms of simplistic exchange energy arguments: despite the presence of nonzero exchange fields, the moments on two of the three Bravais sublattice sites are orientated such that their intraplane exchange energy is zero. This points to a more unconventional reason for the observed moment directions. The most apparent candidates are the unusual localized and extended zero-energy modes within this structure. However, the observation that the sublattice magnetization is close to the spin-only magnitude indicates that the moments are largely frozen in the ordered state. There is therefore an apparent contradiction in the ability of these modes to influence the stability of the observed structure. Further theoretical work is required in order to understand the details of this magnetic structure and the influences that lead to its formation.

VIII. CONCLUSION

In this paper the techniques of representational analysis and reverse-Monte Carlo Rietveld refinement have been used to determine the magnetic structures of jarosites that possess long-range magnetic order. In both the cases of the observed propagation vectors $\mathbf{k}=000$ and $\mathbf{k}=00\frac{3}{2}$, only three symmetry-allowed magnetic structures are found, and the basis vectors for the different propagation vectors are in fact identical. Examination of the refined structures shows that the interplane exchange interactions are important in defining the observed magnetic structures. The salt $(H_3O)V_3(SO_4)_2(OH)_6$ is of particular interest as the observed magnetic structure appears to be the consequence of localized and extended zero-energy excitations.

ACKNOWLEDGMENTS

The author is grateful to the Marie-Curie project of the EC and the Royal Society of Chemistry for funding, to the Institut Laue-Langevin for the provision of experimental time, and to T. Hansen for excellent technical support. It is a pleasure also to acknowledge the Grenoble School of Magnetism for their tuition and many stimulating discussions.

APPENDIX: GROUP-THEORY CALCULATIONS

1. Space-group settings and notation

There has been much comment made of the preference for using primitive cells as the crystallographic frame for the group-theory calculations that make up representational analysis.[23,24,33–38] While this leads to a reduction in possible confusion, particularly over the correct propagation vector, it is certainly not necessary and the calculations are valid for any lattice setting, given that its particular translational symmetry is correctly taken into account. Thus, the nonprimitive space groups more commonly used by crystallographers can be directly used. To demonstrate this, the calculations presented have been made using the hexagonal setting of the $R\bar{3}m$ space group rather than the primitive rhombohedral description. This setting has the additional advantage of retaining the coplanar symmetry of the *kagomé* lattice. Opera-

TABLE V. Symmetry elements of the space group $R\bar{3}m$. The notations used are of the International Tables II (Ref. 42), where the elements are separated into rotation and translation components, and the *Jones faithful representations* of the rotation parts. The latter corresponds to the vector formed from the operation of the rotation part of the element on position (x,y,z).

Element number	IT notation	Jones symbol	Rotation matrix (h)
$g1$	1 (0 0 0)	x,y,z	$\begin{pmatrix}1&0&0\\0&1&0\\0&0&1\end{pmatrix}$
$g2$	3^+ (0 0 0)	$\bar{y},x-y,z$	$\begin{pmatrix}0&\bar{1}&0\\1&\bar{1}&0\\0&0&1\end{pmatrix}$
$g3$	3^- (0 0 0)	$y-x,\bar{x},z$	$\begin{pmatrix}\bar{1}&1&0\\\bar{1}&0&0\\0&0&1\end{pmatrix}$
$g4$	2 (0 0 0)	$y,x,\bar{z}$	$\begin{pmatrix}0&1&0\\1&0&0\\0&0&\bar{1}\end{pmatrix}$
$g5$	2 (0 0 0)	$x-y,\bar{y},\bar{z}$	$\begin{pmatrix}1&\bar{1}&0\\0&\bar{1}&0\\0&0&\bar{1}\end{pmatrix}$
$g6$	2 (0 0 0)	$-x,y-x,\bar{z}$	$\begin{pmatrix}\bar{1}&0&0\\\bar{1}&1&0\\0&0&\bar{1}\end{pmatrix}$
$g7$	$\bar{1}$ (0 0 0)	$\bar{x},\bar{y},\bar{z}$	$\begin{pmatrix}\bar{1}&0&0\\0&\bar{1}&0\\0&0&\bar{1}\end{pmatrix}$
$g8$	$\bar{3}^+$ (0 0 0)	$y,y-x,\bar{z}$	$\begin{pmatrix}0&1&0\\\bar{1}&1&0\\0&0&\bar{1}\end{pmatrix}$
$g9$	$\bar{3}$ (0 0 0)	$x-y,x,\bar{z}$	$\begin{pmatrix}1&\bar{1}&0\\1&0&0\\0&0&\bar{1}\end{pmatrix}$
$g10$	m (0 0 0)	$\bar{y},\bar{x},z$	$\begin{pmatrix}0&\bar{1}&0\\\bar{1}&0&0\\0&0&1\end{pmatrix}$
$g11$	m (0 0 0)	$y-x,y,z$	$\begin{pmatrix}\bar{1}&1&0\\0&1&0\\0&0&1\end{pmatrix}$
$g12$	m (0 0 0)	$x,x-y,z$	$\begin{pmatrix}1&0&0\\1&\bar{1}&0\\0&0&1\end{pmatrix}$

tions that involve its three centering translations are not used in these calculations as they lead only to a trivial scaling of the results.

Before entering into the details of the calculations, a word must first be made about the notations used in this work. The historical development of the application of group theory to the determination of magnetic structures has left the present-day reader with an inconsistent array of terms and variables. In this work, clarification is made where possible of the terms used and relations are stated with the other conventions.

In keeping with Kovalev's notation,[39] h and τ are used to symbolize the rotational and translational parts of the symmetry operator g. However, the h labels used for the rotational symmetry elements in this work are not related to those used by Kovalev as the axes, definitions are not the same. To depict the representations an extension is made to the notation used by Bertaut, and a representation a, which is of order b, is depicted with the symbol $\Gamma_a^{(b)}$.

The program SARAh[17] was used to perform the group-theory calculations. The allowed irreducible representations of the little group are calculated by Zak's induction procedure[40,41] and the basis vectors then calculated as described in the following sections.

2. The irreducible representations

In general, for a given propagation vector $\mathbf{k}$, we find that some of the operators $g=\{h|\tau\}$ of the space group G_0 leave it invariant while others transform it into an equivalent vector that differs by some arbitrary translation of the reciprocal lattice $\mathbf{b}$ according to

$$\mathbf{k}h=\mathbf{k}+\mathbf{b}. \tag{A1}$$

This set of elements make up the so-called little group $G_\mathbf{k}$, which is a subgroup of G_0. The irreducible representations of this little group are given by the symbol Γ_ν, where ν is the label of the irreducible representation, and the matrix that corresponds to the symmetry element g is labeled by $d_\nu^\mathbf{k}(g)$.

The space group $R\bar{3}m$ contains 12 symmetry operators. These are listed in Table V using a number of different conventions. The jarosite systems make up a particularly interesting example as the observed propagation vectors $\mathbf{k}=000$ and $\mathbf{k}=00\frac{3}{2}$ (in the hexagonal dual basis settings) possess the same irreducible representations. This is because $\mathbf{k}=00\frac{3}{2}$ corresponds to a symmetry point of the Brillouin zone and so all elements of the group G_0 are present in the little group of the propagation vector $G_\mathbf{k}$. The irreducible representations of the little group are given in Tables VI and VII.

As Table VII shows, the second-order representations Γ_5 and Γ_6 have the same elements for symmetry operations 1–6 and are related by a factor of (-1) for the operations 7–12.

These irreducible representations may be verified against tabulated values of the projective (or ''loaded'') representations d_ν^{pr}, given in works such as those by Bradley and Cracknell[41] and Kovalev.[39] (Particular care must be taken when comparing these values as the work of Kovalev uses an unconventional setting of the hexagonal axes.) These tabulated representations are given for the various point-group symmetries and can be converted into the irreducible representations of the little group $G_\mathbf{k}$ of the propagation vector $\mathbf{k}$ by the multiplication of a phase factor

$$d_\nu=d_\nu^{pr}\exp(-2\pi\mathbf{k}\cdot\tau), \tag{A2}$$

where τ is the translation part of the symmetry operator to which d_ν is associated.

TABLE VI. First-order irreducible representations for the group D_{3d}^5 for the vectors $\mathbf{k}=000$ and $\mathbf{k}=00\frac{3}{2}$.

	$h1$	$h2$	$h3$	$h4$	$h5$	$h6$	$h7$	$h8$	$h9$	$h10$	$h11$	$h12$
Γ_1	1	1	1	1	1	1	1	1	1	1	1	1
Γ_2	1	1	1	1	1	1	−1	−1	−1	−1	−1	−1
Γ_3	1	1	1	−1	−1	−1	1	1	1	−1	−1	−1
Γ_4	1	1	1	−1	−1	−1	−1	−1	−1	1	1	1

While the presented two-dimensional representations are complex, Herring's criterion [Eq. (A18)] indicates that the representations proper are real:[24]

$$\eta=\frac{1}{n(G_{\mathbf{k}})}\sum_{h:\,\mathbf{k}\mapsto-\mathbf{k}}\chi_\nu(h^2)=\begin{cases}+1 & \text{if } d^{\mathbf{k}\nu} \text{ is real,}\\ 0 & \text{if } d^{\mathbf{k}\nu} \text{ is complex and } d^{\mathbf{k}\nu}\neq(d^{\mathbf{k}\nu})^*,\\ -1 & \text{if } d^{\mathbf{k}\nu} \text{ is complex and } d^{\mathbf{k}\nu}\sim(d^{\mathbf{k}\nu})^*.\end{cases} \tag{A3}$$

Here, ν is the index of the representation under investigation, and the summation is extended over all elements $h\in G_{\mathbf{k}}$, which transform the vector $\mathbf{k}$ into a vector equivalent to $-\mathbf{k}$. $\chi_\nu(h^2)$ is the character of the representation of the element that is the square of h. As in both the cases $\mathbf{k}=000$ and $\mathbf{k}=00\frac{3}{2}$, the vectors $\mathbf{k}$ and $-\mathbf{k}$ are identical, the sum is over all the elements of $G_{\mathbf{k}}$, and so $\eta=1$.

Rather than make these complex representations real by a unitary rotation, we will continue our calculations with these in complex form for pedagogic reasons in order to demonstrate the application of complex basis vectors.

3. Effect of symmetry element on a moment bearing atom: The magnetic representation

The symmetry operator $g=\{h|\tau\}$ acts on both the position r_j of the atom and on the components α of the axial vector that describes the moment. The combination of these two results are described by the magnetic representation Γ. In the following section we will examine these two effects separately.

a. Effect of symmetry element on atom positions: The permutation representation

The operation that sends r_j in the *zero*th cell to r_i in the *p*th cell can be symbolically stated as

$$g(j_0)\rightarrow(i_p). \tag{A4}$$

In other terms, the effect of a symmetry operation g is to permute the column matrix of atom labels $\mathbf{P}$,

$$g(\mathbf{P})\rightarrow\mathbf{P}'. \tag{A5}$$

This operation is governed by a permutation representation Γ_{perm}, which has matrices of order N_A, where N_A is the number of Bravais sublattices (Wyckoff sites) for this atomic position. It is important to note that when a symmetry operation results in an atomic position that is outside the primitive *zero*th cell, a phase factor must be included to relate the generated position to that in the *zero*th cell. The translation that relates atoms of the same Bravais sublattice is necessarily zero or some primitive lattice translation.) This phase is simply given by

$$\phi=-2\pi\mathbf{k}\cdot\mathbf{T}, \tag{A6}$$

where $\mathbf{T}$ is the translation vector which relates the original and generated atoms.

As an example, from Tables VIII and IX we see that the permutation equation for the atoms of the three Bravais sublattices under the $g2=\{3^+|000\}$ operation is

$$\begin{pmatrix}2\cdot\exp(\phi_a)\\ 3\cdot\exp(\phi_b)\\ 1\cdot\exp(\phi_c)\end{pmatrix}=\Gamma_{perm}\begin{pmatrix}1\\ 2\\ 3\end{pmatrix}, \tag{A7}$$

TABLE VII. Second-order irreducible representations for the group D_{3d}^5 for the vectors $\mathbf{k}=000$ and $\mathbf{k}=00\frac{3}{2}$. $\epsilon=\exp(-2\pi/3)$.

	$h1$	$h2$	$h3$	$h4$	$h5$	$h6$
Γ_5,Γ_6	$\begin{matrix}1&0\\0&1\end{matrix}$	$\begin{matrix}\epsilon&0\\0&\epsilon^2\end{matrix}$	$\begin{matrix}\epsilon^2&0\\0&\epsilon\end{matrix}$	$\begin{matrix}0&1\\1&0\end{matrix}$	$\begin{matrix}0&\epsilon^2\\\epsilon&0\end{matrix}$	$\begin{matrix}0&\epsilon\\\epsilon^2&0\end{matrix}$
	$h7$	$h8$	$h9$	$h10$	$h11$	$h12$
Γ_5	$\begin{matrix}-1&0\\0&-1\end{matrix}$	$\begin{matrix}-\epsilon&0\\0&-\epsilon^2\end{matrix}$	$\begin{matrix}-\epsilon^2&0\\0&-\epsilon\end{matrix}$	$\begin{matrix}0&-1\\-1&0\end{matrix}$	$\begin{matrix}0&-\epsilon^2\\-\epsilon&0\end{matrix}$	$\begin{matrix}0&-\epsilon\\-\epsilon^2&0\end{matrix}$
Γ_6	$\begin{matrix}1&0\\0&1\end{matrix}$	$\begin{matrix}\epsilon&0\\0&\epsilon^2\end{matrix}$	$\begin{matrix}\epsilon^2&0\\0&\epsilon\end{matrix}$	$\begin{matrix}0&1\\1&0\end{matrix}$	$\begin{matrix}0&\epsilon^2\\\epsilon&0\end{matrix}$	$\begin{matrix}0&\epsilon\\\epsilon^2&0\end{matrix}$

TABLE VIII. The permutation of B^{3+} atoms (at position $9d$) and the transformation of the axial components of the moment under the different symmetry operators of the $R\bar{3}m$ space group (point group D_{3d}^5) for $\mathbf{k}=000$. The characters of the representations Γ_{perm} and $\tilde{V}$ are given.

Element	$g=\{h\|\tau\}$		Atoms			χ_{perm}	Axial-vector components			$\chi_{\tilde{V}}$
			1	2	3		m_x	m_y	m_z	
$g1$	$\{1$	$\vert\ 0\ 0\ 0\}$	1	2	3	3	m_x	m_y	m_z	3
$g2$	$\{3^+$	$\vert\ 0\ 0\ 0\}$	2	3	1	0	$-m_y$	m_x-m_y	m_z	0
$g3$	$\{3^-$	$\vert\ 0\ 0\ 0\}$	3	1	2	0	$-m_x+m_y$	$-m_x$	m_z	0
$g4$	$\{2$	$\vert\ 0\ 0\ 0\}$	1	3	2	1	m_y	m_x	$-m_z$	-1
$g5$	$\{2$	$\vert\ 0\ 0\ 0\}$	3	2	1	1	m_x-m_y	$-m_y$	$-m_z$	-1
$g6$	$\{2$	$\vert\ 0\ 0\ 0\}$	2	1	3	1	$-m_x$	m_y-m_x	$-m_z$	-1
$g7$	$\{\bar{1}$	$\vert\ 0\ 0\ 0\}$	1	2	3	3	m_x	m_y	m_z	-3
$g8$	$\{\bar{3}^+$	$\vert\ 0\ 0\ 0\}$	2	3	1	0	$-m_y$	m_x-m_y	m_z	0
$g9$	$\{\bar{3}^-$	$\vert\ 0\ 0\ 0\}$	3	1	2	0	m_y-m_x	$-m_x$	m_z	0
$g10$	{m	$\vert\ 0\ 0\ 0\}$	1	3	2	1	m_y	m_x	$-m_z$	-1
$g11$	{m	$\vert\ 0\ 0\ 0\}$	3	2	1	1	m_x-m_y	$-m_y$	$-m_z$	-1
$g12$	{m	$\vert\ 0\ 0\ 0\}$	2	1	3	1	$-m_x$	m_y-m_x	$-m_z$	-1

where the atomic positions follow the labeling $1=(\frac{1}{2}\frac{1}{2}\frac{1}{2})$, $2=(\frac{1}{2}0\frac{1}{2})$, $3=(0\frac{1}{2}\frac{1}{2})$. For the operation $g2=\{3^+|000\}$, $\phi_a=\phi_b=\phi_c=0$ for both $\mathbf{k}=000$ and $\mathbf{k}=00\frac{3}{2}$. The permutation representation is therefore given by

$$\Gamma_{perm}^{\{3^+|000\}}=\begin{pmatrix}0&1&0\\0&0&1\\1&0&0\end{pmatrix}. \tag{A8}$$

The character of this representation χ_{perm} for each symmetry operator is then simply the sum of the phases $\phi(g)$ for the atoms that are transformed into an equivalent atom under a symmetry operation, and so for both the propagation vectors, $\chi_{perm}^{\{3^+|000\}}=0$.

b. Effect of symmetry element on moment vectors: The axial-vector representation

The second effect of this symmetry operation is to transform the spin components with index α ($\alpha=x,y,z$) of the reference spin j into the index α' of the atom at r_i.[36] These transformations are described by the axial-vector representation $\tilde{V}$, the character of which is given by

$$\chi_{\tilde{V}}^h=\mathrm{tr}(R_{ab}^h)\,\delta_h=\sum_{a=b}R_{ab}^h\,\delta_h\,, \tag{A9}$$

where R_{ab}^h refers to a specific element a,b of the rotation matrix h, and δ_h represents the determinant of the rotation matrix R^h, and takes into account that the magnetic moment is not reversed by the inversion operation. This arises as a magnetic moment is described by an axial vector, rather than

TABLE IX. The permutation of B^{3+} atoms (at position $9d$) and the transformation of the axial components of the moment under the different symmetry operators of the $R\bar{3}m$ space group (point group D_{3d}^5) for $\mathbf{k}=00\frac{3}{2}$. The characters of the representations Γ_{perm} and $\tilde{V}$ are given.

Element	$g=\{h\|\tau\}$		Atoms			χ_{perm}	Axial- vector components			$\chi_{\tilde{V}}$
			1	2	3		m_x	m_y	m_z	
$g1$	$\{1$	$\vert\ 0\ 0\ 0\}$	1	2	3	3	m_x	m_y	m_z	3
$g2$	$\{3^+$	$\vert\ 0\ 0\ 0\}$	2	3	1	0	$-m_y$	m_x-m_y	m_z	0
$g3$	$\{3^-$	$\vert\ 0\ 0\ 0\}$	3	1	2	0	$-m_x+m_y$	$-m_x$	m_z	0
$g4$	$\{2$	$\vert\ 0\ 0\ 0\}$	-1	-3	-2	-1	m_y	m_x	$-m_z$	-1
$g5$	$\{2$	$\vert\ 0\ 0\ 0\}$	-3	-2	-1	-1	m_x-m_y	$-m_y$	$-m_z$	-1
$g6$	$\{2$	$\vert\ 0\ 0\ 0\}$	-2	-1	-3	-1	$-m_x$	$-m_x+m_y$	$-m_z$	-1
$g7$	$\{\bar{1}$	$\vert\ 0\ 0\ 0\}$	-1	-2	-3	-3	m_x	m_y	m_z	-3
$g8$	$\{\bar{3}^+$	$\vert\ 0\ 0\ 0\}$	-2	-3	-1	0	$-m_y$	m_x-m_y	m_z	0
$g9$	$\{\bar{3}^-$	$\vert\ 0\ 0\ 0\}$	-3	-1	-2	0	$-m_x+m_y$	$-m_x$	m_z	0
$g10$	{m	$\vert\ 0\ 0\ 0\}$	1	3	2	1	m_y	m_x	$-m_z$	-1
$g11$	{m	$\vert\ 0\ 0\ 0\}$	3	2	1	1	m_x-m_y	$-m_y$	$-m_z$	-1
$g12$	{m	$\vert\ 0\ 0\ 0\}$	2	1	3	1	$-m_x$	$-m_x+m_y$	$-m_z$	-1

by a polar vector. δ_h has the value of $+1$ for a proper and -1 for an improper rotation. The operation of $h(3^+)$ on the moment vector $\vec{M}=(m_x m_y m_z)$ therefore gives

$$R(3^+)\vec{M}=\delta_h\begin{pmatrix}0&-1&0\\1&-1&0\\0&0&1\end{pmatrix}\begin{pmatrix}m_x\\m_y\\m_z\end{pmatrix} \tag{A10}$$

$$=1\begin{pmatrix}-m_y\\m_x-m_y\\m_z\end{pmatrix}. \tag{A11}$$

As 3^+ is a proper rotation, $\delta(3^+)=1$ and the character of $\tilde{V}$ for $h(3^+)$ is $\chi_{\tilde{V}}^{3^+}=0$.

c. The magnetic representation Γ

As already stated, the magnetic representation Γ describes both the result of the symmetry operation on the atomic positions and on the axial vectors that describe the magnetic moments. These effects are independent, and consequentially the magnetic representation is given by their direct product[36,23,33,24]

$$\Gamma=\tilde{V}\times\Gamma_{perm}. \tag{A12}$$

Or, in terms of the matrices for the representations themselves,

$$D^{\Gamma}_{(h,\tau_h)}=D^{\tilde{V}}_{(h)}\times D^{\Gamma_{perm}}_{(h,\tau_h)}. \tag{A13}$$

Their characters are therefore related according to

$$\chi_{\Gamma}=\chi_{\tilde{V}}\times\chi_{perm}. \tag{A14}$$

4. Reduction of the representation Γ

The magnetic representation for a particular site can be decomposed into contributions from the irreducible representations of the little group

$$\Gamma=\sum_{\nu} n_{\nu}\Gamma_{\nu}, \tag{A15}$$

where n_μ is the number of times the irreducible representation Γ_μ appears in the magnetic representation Γ,

$$n_{\nu}=\frac{1}{n(G_k)}\sum_{h\in G_k}\chi_{\Gamma}(h)\chi_{\Gamma^*_{\nu}}(h). \tag{A16}$$

Here χ^{Γ} is the character of the magnetic space group and χ^{Γ}_{ν} is the character of the irreducible representation with index ν.

5. Calculation of the basis vectors Ψ

The μ unique basis vectors ψ_ν that transform according to the μ dimensional irreducible representation Γ^{μ}_{ν} are projected out of any given row of the representation matrix D_ν using the projection operator formula[41]

$$\psi^{i\lambda}_{\nu}=\sum_{h\in G_k} D^{\lambda *}_{(\nu)}\sum_{i}\ \delta_{i,gi}\delta_h R^h\psi^{i\alpha}. \tag{A17}$$

The summation is over the rotational parts of the symmetry elements of the little group $G_{\mathbf{k}}$. ψ is a spin component that we represent by a column matrix $\psi(r)$.

In our calculations the μ elements are those that correspond to the first column of the matrix of D_ν. As for each element labeled $\lambda=1,\ldots,\mu$, three components α are projected out, and there are in total 3μ projected components. The number of unique projected components for a representation is of course the same as calculated using Eq. (A16).

6. Refinement of basis vectors mixing coefficients

Following the Landau theory of a second-order phase transition, any linear combination of basis vectors within the representation that becomes critical is necessarily a symmetry-allowed basis vector. The atomic spin on a particular atom S^i is therefore most generally given by the sum of the basis vectors for a particular irreducible representation

$$S^i=\sum_{\nu} C^i_{\nu}\psi^i_{\nu}, \tag{A18}$$

where C^{ν}_{i} is the mixing coefficient for atom i of the basis vector ν. In refining the orientation of an atomic moment, we are in effect refining the mixing coefficients C^{ν}_{i} of the basis vectors within the irreducible representation being examined. The number of variables in the refinement is simply the number of unique basis vectors that transform according to a given representation, i.e., $n_\nu\mu$.

[1] For recent reviews, see J.E. Greedan, *Proceedings of Materials Discussion 3* [J. Mater. Chem. (to be published)]; A. P. Ramirez, *Handbook of Magnetic Materials* (North-Holland, Amsterdam, in press).

[2] M.G. Townsend, G. Longworth, and E. Roudaut, Phys. Rev. B **33**, 4919 (1986).

[3] T. Inami, S. Maegawa, and M. Takano, J. Magn. Magn. Mater. **177**, 752 (1998).

[4] T. Inami, M. Nishiyama, S. Maegawa, and Y. Oka, Phys. Rev. B **61**, 12 181 (2000).

[5] A.S. Wills, A. Harrison, C. Ritter, and R.I. Smith, Phys. Rev. B **61**, 6156 (2000).

[6] S.H. Lee, C. Broholm, M.F. Collins, L. Heller, A.P. Ramirez, Ch. Kloc, E. Bucher, R.W. Erwin, and N. Lacevic, Phys. Rev. B **56**, 8091 (1997).

[7] A.S. Wills and A. Harrison, J. Chem. Soc., Faraday Trans. **92**, 2161 (1996).

[8] A.S. Wills, A. Harrison, S.A.M. Mentink, T.E. Mason, and Z. Tun, Europhys. Lett. **42**, 325 (1998).

[9] A.S. Wills, V. Dupuis, E. Vincent, J. Hammann, and R. Calem-

czuk, Phys. Rev. B **62**, R9264 (2000).
[10] S.A. Earle, A.P. Ramirez, and R.J. Cava, Physica B **262**, 199 (1999).
[11] S.B. Hendricks, Am. Mineral. **22**, 773 (1937).
[12] A. S. Wills, Ph.D. thesis, The University of Edinburgh, 1997.
[13] J.E. Dutrizac and S. Kaiman, Can. Mineral. **14**, 151 (1976).
[14] J.T. Szymanski, Can. Mineral. **23**, 659 (1985).
[15] A.S. Wills, A. Harrison, and T. Hansen (unpublished).
[16] A.C. Larson and R.B. von Dreele, GSAS, General Structure Analysis System (LANSCE, Los Alamos National Laboratory, Los Alamos, 1994).
[17] A.S. Wills, Physica B **276-278**, 680 (2000); SARA*h*, Simulated Annealing and Representational Analysis. Programs available from ftp.ill.fr/pub/dif/sarah/.
[18] R.L. McGreevy, in *Structural Modelling in Inorganic Crystallography*, edited by R.A. Catlow (Academic Press, New York, 1997).
[19] E.F. Shender, V.B. Cerepanov, P.C.W. Holdsworth, and A.J. Berlinsky, Phys. Rev. Lett. **70**, 3812 (1993).
[20] C. Zeng and V. Elser, Phys. Rev. B **42**, 8436 (1990).
[21] A.B. Harris, C. Kallin, and A.J. Berlinsky, Phys. Rev. B **45**, 2899 (1992).
[22] J. Rossat-Mignod, in *Methods in Experimental Physics*, edited by K. Sköld and D.L. Price (Academic Press, New York, 1987).
[23] E.F. Bertaut, J. Magn. Magn. Mater. **24**, 267 (1981).
[24] Yu.A. Izymov, V.E. Naish, and R.P. Ozerov, *Neutron Diffraction of Magnetic Materials* (Consultants Bureau, New York, 1991).
[25] M. Nishiyama, T. Morimoto, S. Maegawa, T. Inami, and Y. Oka, *Proceedings of Highly Frustrated Magnetism 2000* [Can. J. Phys. (to be published)].
[26] T. Moriya, Phys. Rev. **120**, 91 (1960).
[27] J. Frunzke, T. Hansen, A. Harrison, J. S. Lord, G.S. Oakley, D. Visser, and A.S. Wills, J. Mater. Chem. (to be published).
[28] E. Lelievre-Berna, A. Harrison, G. Oakley, and D. Visser, Annual Report of the Institut Laue-Langevin for 1999, No. Expt. 5-61-37 2000 (unpublished).
[29] J. Villain, R. Bidaux, J.-P. Carton, and R. Conte, J. Phys. (Paris) **41**, 1263 (1980).
[30] C.L. Henley, Phys. Rev. Lett. **62**, 2056 (1989).
[31] J.T. Chalker, P.C.W. Holdsworth, and E.F. Shender, Phys. Rev. Lett. **68**, 855 (1992).
[32] A.S. Wills, *Proceedings of Highly Frustrated Magnetism 2000* [Can. J. Phys. (to be published)].
[33] Yu.A. Izyumov and V.E. Naish, J. Magn. Magn. Mater. **12**, 239 (1979).
[34] E.F. Bertaut, J. Appl. Phys. **33**, 1138 (1962).
[35] E.F. Bertaut, Acta Crystallogr., Sect. A: Cryst. Phys., Diffr., Theor. Gen. Crystallogr. **A24**, 217 (1968).
[36] E.F. Bertaut, J. Phys. (Paris), Colloq. **C1**, 462 (1971).
[37] Yu.A. Izyumov and V.E. Naish, J. Magn. Magn. Mater. **12**, 249 (1979).
[38] Yu.A. Izyumov and V.E. Naish, J. Magn. Magn. Mater. **13**, 267 (1979).
[39] O.V. Kovalev, *Irreducible Representations of the Space Groups* (Gordon and Breach, New York, 1961).
[40] J. Zak, J. Math. Phys. **1**, 165 (1960).
[41] C.J. Bradley and A.P. Cracknell, *The Mathematical Theory of Symmetry in Solids* (Clarendon Press, Oxford, 1972).
[42] *International Tables for Crystallography*, edited by T. Hahn (Kluwer Academic Publishers, Dordrecht, 1996).